THE ASTROPHYSICAL JOURNAL, 229:891–908, 1979 May 1

A HIGH-RESOLUTION STUDY OF THE ABSORPTION SPECTRUM OF PKS 2126−158

PETER J YOUNG AND WALLACE L. W. SARGENT
Hale Observatories, California Institute of Technology, Carnegie Institution of Washington
A. BOKSENBERG
Department of Physics and Astronomy, University College London
AND
R. F. CARSWELL AND J. A. J. WHELAN
Institute of Astronomy, Cambridge University
Received 1978 July 5; accepted 1978 November 21

ABSTRACT

Observations of the QSO PKS 2126−158 (z_{em} = 3.280) at 0.8 Å resolution from 4153 Å to 6807 Å reveal 113 absorption lines. There are two certain absorption-line systems at z_{abs} = 2.6381 and 2.7685, and a possible third system at z_{abs} = 2.3938. The ions H I, C II, C IV, O I, Al II, Si II, Si III, Si IV, and Fe II are observed in these systems; no excited fine-structure lines Si II* are seen, but C II* is almost certainly present in the z_{abs} = 2.7685 system. These three systems lead to the identification of all 12 lines longward of the Lα emission line. However, only 22 out of 101 absorption lines shortward of Lα are thereby identified.

Among the otherwise unidentified lines shortward of Lα emission we find at most three clear Lα/β pairs. A cross-correlation between the regions of spectrum below Lα and Lβ emission, respectively, shows a strong peak at the Lα/β ratio. The peak has the strength expected on the hypothesis that $\gtrsim 90\%$ of the lines shortward of Lα emission are Lα absorptions with the corresponding Lβ absorption buried in the noise.

The analysis of the spectrum of PKS 2126−158 is used to develop criteria for defining particular types of redshift systems which can then form a basis for statistical analyses of the distribution of absorption systems with redshift in QSOs generally.

Subject headings: line identifications — quasars

I. INTRODUCTION

The Cerro Tololo objective prism survey (Smith 1975) has led to the discovery of several QSOs brighter than 18 mag and with redshifts $z_{em} \gtrsim 2$ which are ideal for high-resolution studies of absorption lines. Accordingly, when a new version of the University College London Image Photon Counting System (Boksenberg 1972) was installed by several of the present authors on the Anglo-Australian telescope in 1976 November, a prime goal was to obtain a homogeneous set of spectra of a sample of the Tololo QSOs. Observations were in fact obtained of five of these objects; these will be described in future papers. However, during the course of these observations we were informed by Jauncey and Peterson of the discovery of a 17.3 mag QSO with z_{em} = 3.27 and identified with the radio source PKS 2126−158 (Jauncey *et al.* 1978*a*, *b*). This object was found by Jauncey *et al.* to have a rich absorption spectrum characteristic of high-redshift QSOs, and we immediately made high-resolution observations, similar to those being made on the Tololo QSOs, as detailed in Table 1. Our measurements covered the wavelength range λλ4150–5520 in two exposures: copies of the data tapes were given to Jauncey *et al.* for their studies of the object. Later, Jauncey *et al.* made available to us their high-resolution observations of the longer-wavelength region λλ5150–6810, as detailed in Table 1.

This paper deals with the analysis of the rich absorption spectrum of PKS 2126−158 revealed by these observations. The main goals were to identify the major absorption redshift systems and also to test whether most of the lines observed shortward of the Lα emission line are single Lα absorption lines, as suggested by Lynds (1971). Moreover, we have attempted to establish a set of uniform criteria, both for the discovery of absorption lines in the data and for their measurement, which can be generally applied to high-resolution observations made with the IPCS to some defined signal-to-noise ratio. In the same spirit, we have devised a classification scheme for absorption redshifts which is designed to enable one to compare the redshift distributions in different quasars in a manner which is as free as possible of observational selection effects. In subsequent work we shall apply these criteria for the selection and identification of lines to the observations of the Tololo QSOs.

In the rest of this paper, § II contains further details of the observational material, and § III is concerned with the identification of the absorption lines in terms of conventional redshift systems. The identification of the many absorption lines shortward of Lα is considered in § IV. The conclusions are listed in § V.

TABLE 1

OBSERVATIONS OF PKS 2126−158

Date	t(sec)	λ-Range (Å)	Pixel Format	Pixel Size(Å)	FWHM (Å)	Rebinned λ-Range	No. Rebinned Points	Mean Count* Level
1976 Nov.	5400	4750-5520	1750x10	0.45	0.87	4745.00-5155.00	1750	130
1976 Nov.	6000	4150-4950	1750x10	0.46	0.72	4153.28-4946.93	2035	60
1977 June	10000	5150-6260	2048x2	0.56	1.05	5175.22-6198.69	2100	60
1977 June	5500	5700-6810	2048x2	0.56	1.05	5693.16-6807.36	2080	30

*Per channel, in continuum away from emission lines.

II. OBSERVATIONS AND PRELIMINARY REDUCTIONS

a) Initial Reductions

The observations of PKS 2126−158 were obtained with the IPCS mounted on the RGO spectrograph at the f/8 Cassegrain focus of the Anglo-Australian 3.9 m telescope. The device was used in a two-dimensional mode to allow simultaneous sky monitoring and accurate subtraction. A 1200 line mm^{-1} grating blazed in first order at λ4600 was used in conjunction with an f/1.67 camera of focal length 25 cm. The resulting dispersion was 25 Å mm^{-1}. The slit width of 1″.5 (=220 μm) projected onto two resolution elements in the detector, each element being 0.45 Å or 0.56 Å on average as indicated in Table 1. The wavelength scale for the spectra covering the region 4153 Å to 6807 Å was established with an argon-copper arc; the unblended lines chosen were fitted in a fully two-dimensional manner with quintic polynomials leaving residuals of <0.1 Å. The QSO data were divided by a flat field and sky subtracted in the manner described in Sargent *et al.* (1978), and subsequently rebinned on a logarithmic wavelength scale with $\Delta\lambda/\lambda = 9.59315 \times 10^{-5}$ (25.78 km s^{-1} per channel). It should be noted that all wavelengths quoted in this paper are as measured in vacuo and have been corrected to heliocentric values.

Four separate scans of PKS 2126−158 were made, as laid out in Table 1. Although the data have significant overlap, the four scans were treated separately for the purposes of compiling line lists to ensure uniformity across the observed region. In Figure 1 we show the data with the absorption lines indicated. The method of choosing these lines is described in § III. It may be seen that the region 5700–6810 Å has a significantly lower count level than do the other three scans.

b) Emission Lines

We measured the wavelengths and equivalent widths of the emission lines in our data by planimetering suitably scaled plots. The center of luminosity of a line was chosen to represent its mean wavelength, since the extreme weakness of the majority of the features prevents accurate measurement of the line peak. Results are given in Table 2 which establish $z_{em} = 3.280 \pm 0.002$, in accord with the value $z_{em} = 3.27$ given by Jauncey *et al.* Shortward of Lα, only the feature Lβ/O VI λ1033 was visible. It was unmeasured due to the density of absorption lines in the region of the spectrum. The modest equivalent widths of Lα and C IV λ1549 in the spectrum of PKS 2126−158 are consistent with the correlation found by Baldwin (1977) between absolute luminosity and equivalent width.

c) Selection of Absorption Lines

Plots of the data similar to Figure 1 were searched for absorption lines by the following procedure. Sup-

TABLE 2

EMISSION LINES IN PKS 2126−158

Ion	Rest Wavelength (Å)	Observed Wavelength (Å)	z_{em}	Observed Equiv. Width (Å)	Rest Frame Equiv. Width (Å)
H I	1216	5201±3	3.278±0.002	350±20	82±5
N V	1240	5306±5	3.278±0.003	14.8±1.0	3.5±0.2
Si II	1264	5410±8	3.280±0.006	9.9±0.6	2.3±0.1
O I	1305	5590±8	3.283±0.006	15.3±1.0	3.6±0.2
Si IV	1397	5981±8	3.281±0.006	71±3	16.6±0.7
C IV	1549	6609±15	3.266±0.010	116±10	27.1±2.3
Mean (excluding C IV 1549)			3.280±0.002		

pose we have digital data with N_i counts in the ith channel. Then we define the position of a line to be

$$\Lambda = \sum_i i(N_c - N_i) \Big/ \sum_i (N_c - N_i) , \qquad (1)$$

where the summations are made over the M_L channels which form the line. (We shall develop later the criteria for determining which depressions in the continuum constitute lines.) The equivalent width, W, of a line is defined by

$$W = \frac{1}{N_c} \sum_i (N_c - N_i) , \qquad (2)$$

where N_c is the count level in the local continuum. According to Poisson counting statistics, the variance in the count level of channel i is given by $\sigma^2(N_i) = N_i + 2N_k$, where N_k is the count level in the sky as subtracted from the data. If the continuum is well defined, the variance in W is given by

$$\sigma^2(N_c W) = N_c{}^2\sigma^2(W) = M_L(N_c + 2N_k) - WN_c , \qquad (3)$$

where M_L is the number of channels involved in the summation of equation (2). To minimize noise, it is clearly profitable to reduce M_L to as small a value as possible, i.e., to set M_L to the full-width zero-intensity of the line. Since it is easier to determine the full-width half-intensity of a line, we computed this and set M_L equal to 2.5 times this value. A Gaussian line has then fallen to 1.3% of the peak strength. Lines with broad wings will then be assigned systematically small values of W. Such wings, however, are not readily distinguishable from undulations in the continuum in the quality of data presented here. The variance in the wavelength determination is given by

$$N_c{}^2 W^2 \sigma^2(\Lambda) = (N_c + 2N_k)(M_L{}^3/12) - N_c W \sigma_L{}^2 , \qquad (4)$$

where

$$N_c W \sigma_L{}^2 = \sum_i (i - \Lambda)^2 (N_c - N_i) .$$

For normal line profiles, $\sigma_L{}^2 = M_L{}^2/12$, and so

$$\sigma^2(\Lambda) \approx [\sigma(W)/W]^2 (M_L{}^2/12) . \qquad (5)$$

The continuum was found by the following procedure. First, strong emission lines were fitted approximately with an appropriate analytic formula and divided out. This left only minor, long-wavelength fluctuations in the data. Then the spectrum was divided into consecutive segments of length 100 channels. The standard deviation, σ, of the total count level in each segment was formed by calculating

$$\mu = \sum_{i=1}^{100} N_i/100$$

and

$$\sigma^2 = \sum_{i=1}^{100} (N_i - \mu)^2/99 .$$

A theoretical standard deviation σ_T was also formed. Thus, if the count level in the jth QSO channel is $n_j{}^{\mathrm{Q}}$, and that in the "sky" is $n_j{}^{\mathrm{s}}$, then

$$N_i = \sum \alpha_j n_j{}^{\mathrm{Q}} - \sum \beta_j n_j{}^{\mathrm{s}}$$

where the factors α_j and β_j allow for the flat-field division and rebinning to a logarithmic scale. Clearly,

$$\sigma^2(N_i) = \sum \alpha_j{}^2 n_j{}^{\mathrm{Q}} + \sum \beta_j{}^2 n_j{}^{\mathrm{s}} ,$$

and we set

$$\sigma_T{}^2 = \sum_{i=1}^{100} \sigma^2(N_i)/100 .$$

Since the spectrum contains deep absorption lines, then, in general, $\sigma > \sigma_T$. In that event we rejected channels, starting with the ones with the smallest count levels, and formed a progression of new values of σ and σ_T, stopping when $\sigma < \sigma_T$. If the number of channels remaining was less than a specified number $N_{\min}$ (which we set equal to 30) then the whole segment was ignored. The continuum level at the mean wavelength (λ) of the points remaining in the segment was deemed to be the mean count level (μ) of those remaining points.

The series of (λ, μ) points from all the remaining data segments were spline-fitted with cubic polynomials and the data were divided by these polynomials so that the "continuum" level everywhere has normalized to unity. (Alternatively, the data may be left alone, and the continuum deemed to be the product of the cubic polynomial spline fit and the "line division" functions mentioned in the first step above.)

This procedure was found to determine continuum levels in regions of heavy line density to an accuracy of 5% in computer-simulated data. One cannot be certain, however, that the continuum level is not depressed by unresolved weak lines, or perturbed by nonstatistical fluctuations in the data.

For lines longward of the Lα emission line it was a straightforward matter to calculate the $\sigma(W)$ value given in equation (3) [except that we used the more accurate $\sigma(N_i)$ as given in the continuum fitting procedure]. To be accepted as real, we required that $W > 4\sigma(W)$. If a line was sought but not found, we give an upper limit $W = 4\sigma(W)$. Since there may be systematic errors in the continuum level, we set $\sigma_c(W) = W/10$, and then $\sigma^2(W) \to \sigma^2(W) + \sigma_c{}^2(W)$. Wavelengths and their standard deviation $\sigma(\Lambda)$ were calculated, and to allow for possible systematic distortions of the wavelength scale, we set $\sigma_\lambda = 0.2$ Å, and $\sigma^2(\Lambda) \to \sigma^2(\Lambda) + \sigma_\lambda{}^2$.

For lines shortward of Lα emission the same procedure was employed except where the congestion of the lines became unduly high. Broad lines with

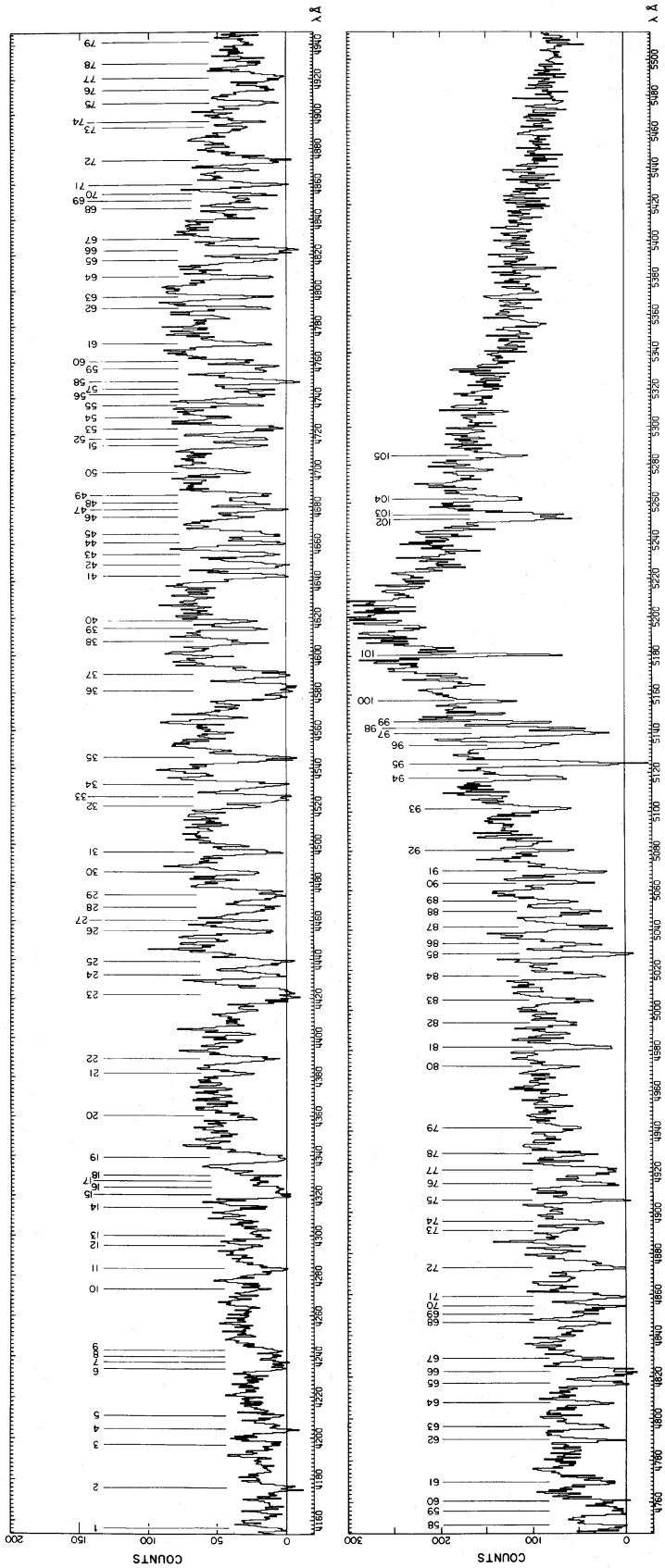

FIG. 1.—Spectrum of PKS 2126−158, showing four overlapping, independent observations covering the range 4153–6807 Å. Each bin is equivalent to 25.78 km s^{-1} (the wavelength axis is logarithmic). The zero intensity level in each observation is indicated by the horizontal lines. The 113 absorption lines listed in Table 3 are marked and labeled.

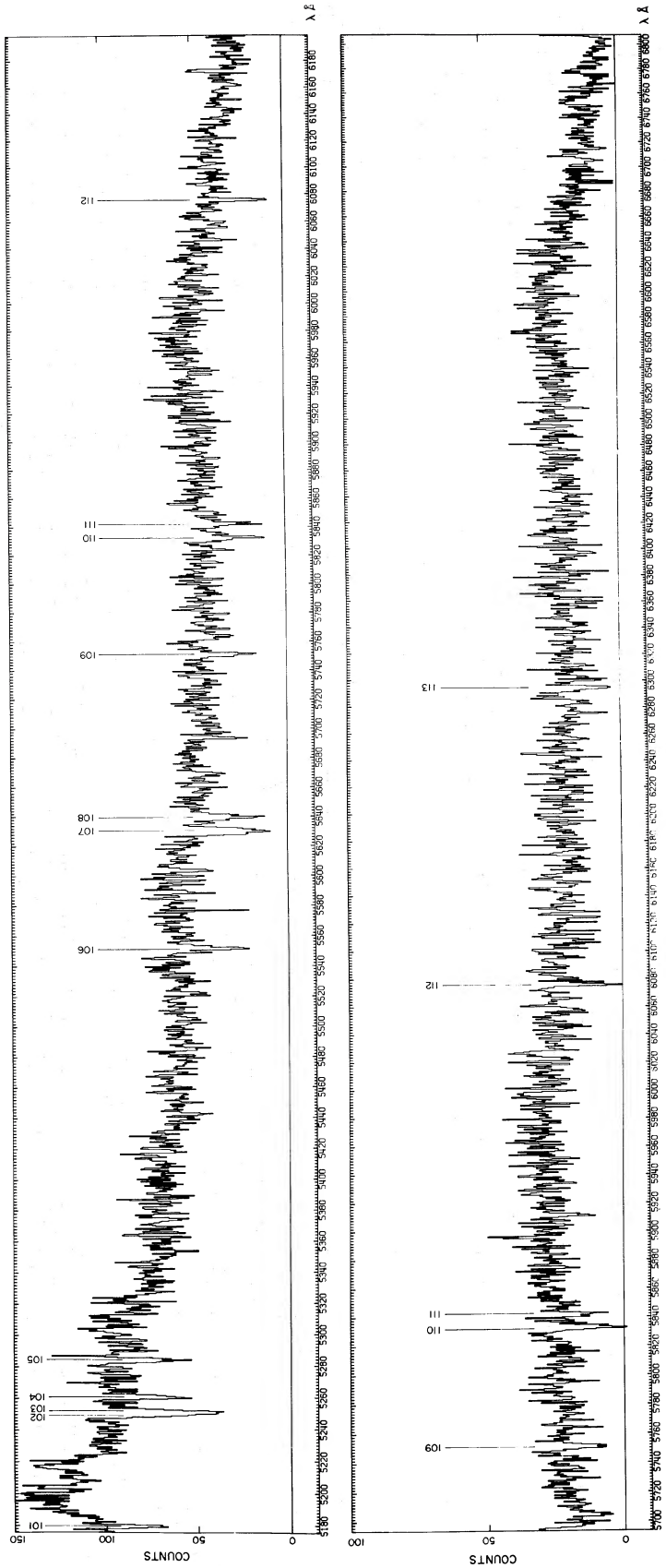

FIG. 1.—*continued*

TABLE 3

PKS 2126−158 ABSORPTION-LINE LIST

n	λ Å	σ(λ) Å	W Å	σ(W) Å	N_c	ID	z(ID)	Comments
1	4156.4	0.2	1.6	0.2	30			
2	4175.9	0.2	4.4	0.4	32			
3	4197.2	0.2	2.1	0.2	42			
4	4205.3	0.3	3.8	0.4	42			
5	4211.2	0.3	2.0	0.4	43			
6	4234.7	0.6	2.2	0.5	47			C1
7	4237.8	0.6	2.9	0.5	47			C1
8	4240.6	0.3	1.0	0.2	48			C1
9	4243.3	0.3	2.2	0.4	48			C1
10	4274.0	0.2	1.0	0.2	56			
11	4283.6	0.2	4.3	0.4	57			
12	4295.0	0.2	1.1	0.2	58			
13	4300.5	0.5	1.8	0.3	60			
14	4314.8	0.2	1.2	0.2	60	FeII(1144)	2.7686	
15	4320.9	0.6	3.1	0.5	66			C2
16	4324.4	0.6	3.0	0.5	66			C2
17	4327.3	0.5	0.9	0.3	67			C2
18	4331.1	0.5	2.0	0.4	67	SiII(1190)	2.6383	C2
19	4339.9	0.2	4.9	0.5	70	SiII(1193)	2.6370	
20	4360.4	0.2	1.5	0.2	72			
21	4382.5	0.2	1.1	0.2	76			
22	4389.9	0.2	2.7	0.3	76	SiIII(1206)	2.6385	
23	4422.6	0.2	8.6	0.9	82	HI(1215)	2.6380	
24	4432.8	0.2	2.9	0.3	84			
25	4439.8	0.2	4.6	0.5	84			
26	4455.3	0.2	2.1	0.2	84			
27	4461.0	0.2	0.7	0.1	84			
28	4467.0	0.3	4.3	0.5	84			
29	4474.3	0.3	5.2	0.6	84			
30	4486.1	0.2	1.5	0.1	83	SiII(1190)	2.7685	
31	4496.7	0.2	2.3	0.2	81	SiII(1193)	2.7684	
32	4520.6	0.3	1.2	0.1	82			
33	4524.9	0.2	4.7	0.5	83			
34	4531.8	0.2	3.6	0.4	84			
35	4546.1	0.2	3.8	0.4	84	SiIII(1206)	2.7680	
36	4581.5	0.2	9.4	0.9	86	HI(1215)	2.7687	
37	4590.8	0.2	5.2	0.5	86			
38	4608.0	0.2	1.9	0.2	86			
39	4615.1	0.2	1.4	0.1	86			
40	4618.9	0.2	1.4	0.1	86			
41	4643.2	0.2	3.6	0.4	87			
42	4649.4	0.2	4.0	0.4	87			
43	4655.1	0.2	2.9	0.3	87			
44	4661.3	0.2	2.9	0.3	87			
45	4665.9	0.2	3.4	0.3	87			
46	4675.0	0.3	0.9	0.2	87			
47	4679.2	0.2	3.0	0.3	87			
48	4683.3	0.2	2.0	0.2	87			
49	4687.3	0.2	2.5	0.3	87			
50	4699.7	0.2	1.7	0.2	85			
51	4714.5	0.2	1.8	0.2	85			
52	4718.0	0.2	1.9	0.2	85			
53	4723.7	0.2	3.4	0.3	83			
54	4730.2	0.2	0.7	0.2	83	SiIV(1393)	2.3938	
55	4736.9	0.2	1.2	0.1	83	OI(1302)	2.6377	
56	4742.4	0.4	2.4	0.4	81			C3
57	4745.5	0.5	1.6	0.3	81	SiII(1304)	2.6381	C3
58	4750.0	0.2	4.1	0.4	80,63	SiII(1260)	2.7686	
59	4756.9	0.2	3.8	0.4	80,72			
60	4761.2	0.2	1.7	0.2	80,74			
61	4771.2	0.2	2.5	0.3	80,90			
62	4791.1	0.2	1.3	0.1	80,90			
63	4797.3	0.2	1.5	0.2	82,92			
64	4808.3	0.2	1.6	0.2	80,90			
65	4817.8	0.2	2.5	0.3	76,88			
66	4823.0	0.2	4.6	0.5	76,88			

TABLE 3—*Continued*

n	λ Å	σ(λ) Å	W Å	σ(W) Å	N_c	ID	z(ID)	Comments
67	4829.6	0.2	1.1	0.1	76,88			
68	4846.9	0.3	1.1	0.2	72,88			
69	4851.1	0.4	1.0	0.3	70,88			C4
70	4854.6	0.4	1.9	0.5	67,88	CII(1334)	2.6377	C4
71	4859.6	0.3	2.5	0.3	65,88	CII*(1335)	2.6388	
72	4874.5	0.2	3.8	0.4	64,87			
73	4892.6	0.2	0.6	0.1	60,87			
74	4896.3	0.3	1.0	0.2	58,87			
75	4906.8	0.2	1.8	0.2	55,87	OI(1302)	2.7682	
76	4915.1	0.2	2.3	0.2	50,90	SiII(1304)	2.7682	
77	4921.3	0.2	4.2	0.4	46,90			
78	4929.5	0.2	1.0	0.1	42,90			
79	4942.2	0.3	1.0	0.2	38,90			
80	4972.8	0.2	0.5	0.1	92			
81	4982.7	0.2	1.9	0.2	95			
82	4994.3	0.2	0.9	0.1	98			
83	5005.7	0.2	1.3	0.2	100			
84	5018.5	0.2	1.8	0.2	104			
85	5028.8	0.2	3.0	0.3	107	CII(1334)	2.7682	
86	5033.4	0.2	1.8	0.2	111	CII*(1335)	2.7688	
87	5042.7	0.2	2.7	0.3	115			
88	5050.0	0.2	2.6	0.3	117			
89	5055.5	0.2	1.4	0.2	118			
90	5064.4	0.2	1.9	0.2	120			
91	5070.7	0.2	3.0	0.3	120	SiIV(1393)	2.6382	
92	5080.9	0.2	1.0	0.2	122			
93	5102.6	0.2	1.8	0.2	144	SiIV(1402)	2.6375	
94	5118.5	0.2	1.5	0.2	158			
95	5125.8	0.2	2.9	0.3	163			
96	5135.0	0.2	1.8	0.2	172			
97	5140.7	0.4	2.3	0.5	177			C5
98	5143.5	0.4	1.6	0.4	178			C5
99	5146.8	0.2	1.1	0.2	184			
100	5157.4	0.2	1.1	0.2	200			
101	5181.5	0.2	1.3	0.1	244,110	SiII(1526)	2.3838	
102	5252.1	0.4	1.7	0.4	178,95	SiIV(1393)	2.7683	C6
103	5254.1	0.4	2.0	0.4	175,95	CIV(1548)	2.3937	C6
104	5263.0	0.2	1.3	0.1	165,90	CIV(1550)	2.3938	
105	5286.1	0.2	0.8	0.1	158,90	SiIV(1402)	2.7683	
106	5554.5	0.2	2.7	0.3	60	SiII(1526)	2.6382	
107	5632.1	0.3	5.4	0.5	53	CIV(1548)	2.6378	
108	5641.8	0.2	3.2	0.3	52	CIV(1550)	2.6380	
109	5753.4	0.2	2.3	0.2	48,24	SiII(1526)	2.7684	
110	5835.0	0.3	3.2	0.4	45,25	CIV(1548)	2.7689	
111	5844.8	0.3	2.2	0.2	45,25	CIV(1550)	2.7690	
112	6078.1	0.3	1.8	0.2	40,26	AlII(1670)	2.6378	
113	6296.5	0.3	2.0	0.2	25	AlII(1670)	2.7685	

NOTES TO TABLE 3

Wavelength region analyzed: 4153–6807 Å.
All wavelengths heliocentric, vacuum values.
N_c = number of counts in continuum near line. Two values given where line measured on two spectra.
Lines which are members of a confused complex (*J*) are denoted *CJ*.

substructure and obvious blends had to be subjectively decomposed into separate lines, which were assigned higher $\sigma(W)$, $\sigma(\Lambda)$ values commensurate with the degree to which they were buried. It was possible to make independent checks on the $\sigma(W)$, $\sigma(\Lambda)$ values by comparing regions of overlapping data.

The resulting 113 lines in the spectrum of PKS 2126−158 are listed in Table 3 with wavelengths rounded to 0.1 Å. A final demand on the strength of a real line was made by insisting it be stronger than any of the spurious (nonstatistical) upward fluctuations that appear in the continuum regions of the spectrum. In some of the spectra such upward fluctuations were of strength 5 σ, thereby leading to a slightly more severe limit. After all these precautions, we are confident that no more than two or three lines in Table 3 are likely to be spurious.

III. ABSORPTION-LINE SYSTEMS

a) Identification of Systems

The redshift systems were fairly obvious because there are three pairs of lines having the separation of

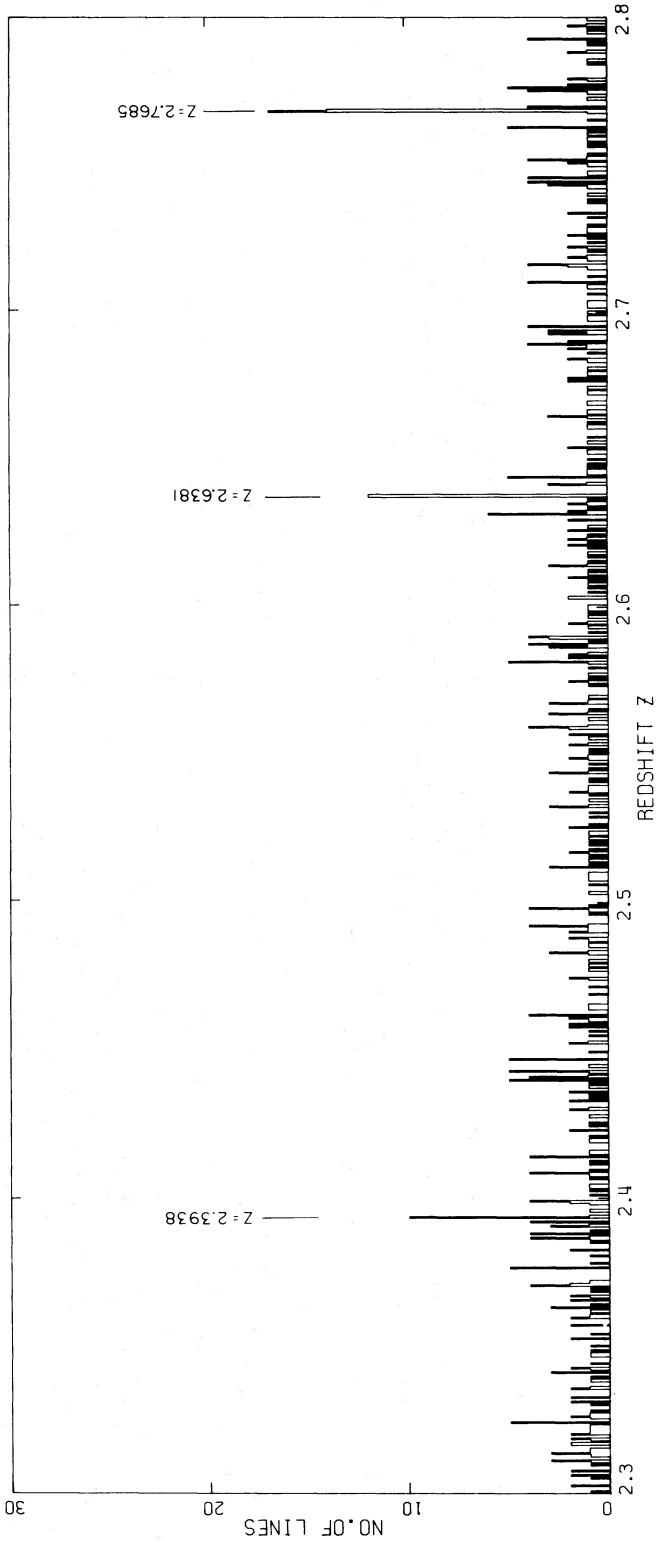

FIG. 2.—Plot of matrix of redshifts z_{ij} formed by dividing observed wavelengths λ_i by laboratory wavelengths Λ_j for a set of 26 "standard" lines. We have binned z_{ij} in intervals $\Delta z = 0.0005$ and plotted the number of z_{ij}'s in each bin. Lines λ_i longward of Lα emission in the QSO are weighted with a factor $n_w = 4$. The three redshift systems found by this procedure are marked.

TABLE 4

LIST OF CANDIDATE LINES

Ion	λ_{vac} (Å)	Ion	λ_{vac} (Å)
*H I	1215.67	*Mg II(2)	2796.35
*H I	1025.72	Aℓ II	1670.81
H I	972.54	Aℓ III(1)	1862.78
H I	949.74	Aℓ III(2)	1854.72
H I	937.80	*Si II	1526.72
C I	1656.92	*Si II	1304.37
C I	1560.31	*Si II	1260.42
C I	1277.15	*Si II(2)	1193.28
C I	1260.75	*Si II(1)	1190.42
C I	945.19	*Si III	1206.51
*C II	1334.53	*Si IV(1)	1402.77
*C II	1036.34	*Si IV(2)	1393.76
C II	903.85	S I	1425.10
C III	977.03	S I	1295.79
*C IV(1)	1550.77	S V	786.48
*C IV(2)	1548.20	S IV(1)	944.52
N V(1)	1242.80	S IV(2)	933.38
N V(2)	1238.81	K I(1)	7701.19
O I	1302.17	K I(2)	7667.12
O I	877.86	*Ca II(1)	3969.65
O III	832.93	*Ca II(2)	3934.83
O III	702.33	Ti II	3384.78
O IV	787.71	Ti II	3242.96
O IV	608.40	Ti II	3230.17
O V	629.73	Ti II	3073.91
O VI(1)	1037.63	Fe I	3861.06
O VI(2)	1031.95	Fe I	3721.05
*Na I(1)	5897.64	Fe I	2523.61
*Na I(2)	5891.66	Fe I	2484.02
Na I(1)	3303.98	*Fe II	2600.18
Na I(2)	3303.37	*Fe II	2586.64
*Mg I	2852.97	*Fe II	2382.76
Mg I	2026.47	*Fe II	2374.46
Mg I	1828.17	*Fe II	2344.21
*Mg II(1)	2803.53	Fe II	1144.94
		Fe III	1122.53

the C IV λλ1548, 1550 doublet among the few lines observed longward of the Lα emission line. A systematic search procedure was adopted, however, in order to find systems in which the principal lines lie shortward of Lα.

The method adopted is essentially that of Bahcall (1968), with some minor modifications. A set of "standard" wavelengths Λ_j (given in Table 4) and a list of observed lines λ_i were used to form a matrix $z_{ij} = \lambda_i/\Lambda_j - 1$. These values of z_{ij} were then cast into bins of size Δz in redshift space, with a weight $w = 1$ if $\lambda_i < \lambda$(Lα emission) and a weight n_w where $n_w > 1$ if $\lambda_i > \lambda_{L\alpha}$. We thus heavily weight lines longward of Lα emission in the QSOs. The function $n(z, \Delta z)$, the total number of z_{ij}'s in the interval z to $z + \Delta z$, with appropriate weighting factor for each z_{ij}, was plotted and searched for peaks in the distribution. If $n^*(z, \Delta z)$ is the average level of this distribution at a particular value of z, then we formed $n = [n_1(z, \Delta z) + n_2(z, \Delta z) - 2n^*(z, \Delta z)]$, for each consecutive pair of channels, and gave the "system" further consideration if we found $n \geq n_F$ where n_F is specified below.

The standard wavelength list included 71 transitions from 600 Å to 10000 Å and thus covered a range of redshifts from $z = -0.5$ to $z = 11.0$. In Table 4 it can be seen that we have given 26 lines asterisks. These form a "short list" with which separate runs are made (which yield far fewer "spurious" candidates). It is rare that lines not in this "short list" have been observed in QSO absorption spectra which are of small chance probability, unless that system is very strong (e.g., $z_{abs} = 2.3095$ in PHL 957). The ease with which an absorption system can be found is far from being uniform with z because of the distribution of strong standard lines. In particular, it is hard to find systems if the C IV λλ1548, 1550 or Mg II λλ2796, 2803 doublets do not fall in the observed spectral range. Moreover, the expected weakness of the Ca II λλ3934, 3969 and Na I λλ5891, 5897 doublets makes it difficult to detect systems near zero redshift.

In our investigation we used the values $\Delta z = 0.0005$, $n_W = 4$, and $n_F = 6$ which successfully removed most of the spurious systems. The value n_W is the ratio of line densities shortward and longward of Lα emission. This ratio is actually 13 in PKS 2126−158, but a value of 4 was chosen by taking the ratio for all lines in a sample of five QSOs which we shall report on in later papers. This allows a uniform analysis of all objects. The value of n_F was determined by trial and error in order that a reasonable number of systems to be further checked could be obtained. Around 20 systems would then present themselves. Of the systems chosen by the computer program, a check was made to ensure that doublet ratios were correct and that line strengths among a single ion were consistent with their f-values. This allows the acceptance of systems with only a few lines, if they are longward of Lα, but demands many lines if they are shortward of Lα. A discussion of the probability analysis involved is given later on in the paper.

In Figure 2 we show a plot of $n(z, \Delta z)$, as a function of z, over the range $2.3 \leq z \leq 2.8$. This plot was made using the "short list" rather than the full 71 transitions in Table 4. This shows the significance of the peaks in $n(z, \Delta z)$ at the redshifts of the three absorption-line systems which survived the stringent tests described above. They are listed in Table 5. We now discuss them individually.

$z_{abs} = 2.3938$.—A possible four-line system with C IV, Si II, and Si IV, of which the C IV is longward of Lα: however, the stronger line of the doublet is blended with Si IV in one of the other systems, $z_{abs} = 2.7685$. Several expected strong lines—Lα and Si III λ1206, for example—lie just outside the observed range, and others (Si II λ1260, Si II λ1304) fall in regions thick with lines or in regions of poor signal-to-noise ratio. The weaker member of the Si IV doublet, λ1402, would be too weak to be visible. Thus this system is not completely convincing. It would become far stronger if the expected Lα line at λ4125.7 were observed in new observations. A possible line is seen in the low-resolution data of Jauncey *et al.* (1978*a*).

$z_{abs} = 2.6381$.—A certain system with 14 lines, of which four are longward of Lα. The Si II λ1193 line is probably blended, since it is rather too strong and has a wavelength discrepancy of −1.30 Å. Four lines

TABLE 5

PKS 2126−158: Absorption-Line Systems

	Ion	Rest λ (Å)	λ(1+z_{abs}) (Å)	Obs. λ (Å)	O-C (Å)	z_{abs}	W (Å)	W/(1+z) (Å)	Comments
1	CIV(1)	1550.77	5262.99	5263.02	+0.03	2.3938	1.3	0.39	
	CIV(2)	1548.20	5254.27	5254.11	-0.16	2.3937	2.0	0.59	
	SiII	1526.72	5181.37	5181.45	+0.08	2.3938	1.3	0.39	
	SiIV	1393.76	4730.14	4730.18	+0.04	2.3938	0.7	0.21	
					$\langle z_{abs} \rangle$ =	2.3938			
2	HI	1215.67	4422.67	4422.55	-0.12	2.6380	8.6	2.4	
	CI	1656.92	6028.04	...	...	...	<0.8	<0.2	
	CII(J=1/2)	1334.53	4855.09	4854.58	-0.51	2.6377	1.9	0.52	
	CII*(J=3/2)	1335.68	4859.34	4859.60	+0.26	2.6388	2.5	0.68	Possibly bogus
	CIV(1)	1550.67	5641.78	5641.77	-0.01	2.6380	3.2	0.88	
	CIV(2)	1548.20	5632.43	5632.11	-0.32	2.6378	5.4	1.5	
	OI	1302.17	4737.36	4736.89	-0.47	2.6377	1.2	0.33	
	AlII	1670.81	6078.49	6078.09	-0.40	2.6378	1.8	0.50	
	SiII(J=1/2)	1526.72	5554.29	5554.45	+0.16	2.6382	2.7	0.74	
	SiII*(J=3/2)	1533.44	5578.81	...	...	...	<0.9	<0.25	
	SiII	1304.37	4745.36	4745.49	+0.12	2.6381	1.6	0.45	
	SiII*	1309.28	4763.29	...	...	...	<0.5	<0.15	
	SiII(2)	1193.28	4341.21	4339.91	-1.30	2.6370	4.9	1.4	Probably blended
	SiII(1)	1190.42	4330.81	4331.13	+0.32	2.6383	2.0	0.5	
	SiII*	1197.42	4356.33	...	...	...	<0.7	<0.2	
	SiII*	1194.50	4345.71	...	...	...	<0.5	<0.15	
	SiIII	1206.51	4389.34	4389.88	+0.53	2.6385	2.7	0.73	
	SiIV(1)	1402.77	5103.35	5102.60	-0.75	2.6375	1.8	0.48	
	SiIV(2)	1393.76	5070.57	5070.74	+0.17	2.6382	3.0	0.81	
					$\langle z_{abs} \rangle$ =	2.6381			
3	HI	1215.67	4581.20	4581.51	+0.31	2.7687	9.4	2.5	
	CI	1656.92	6244.10	...	...	...	<1.5	<0.4	
	CII(J=1/2)	1334.53	5029.11	5028.83	-0.28	2.7682	3.0	0.79	
	CII*(J=3/2)	1335.68	5033.51	5033.43	-0.07	2.7688	1.8	0.48	
	CIV(1)	1550.77	5844.00	5844.82	+0.81	2.7690	2.2	0.58	
	CIV(2)	1548.20	5834.32	5835.02	+0.70	2.7689	3.2	0.85	
	OI	1302.17	4907.17	4906.78	-0.39	2.7682	1.8	0.48	
	AlII	1670.81	6296.37	6296.46	+0.09	2.7685	2.0	0.53	
	SiII(J=1/2)	1526.72	5753.38	5753.36	-0.02	2.7684	2.3	0.60	
	SiII*(J=3/2)	1533.44	5778.77	...	...	...	<0.8	<0.2	
	SiII	1304.37	4915.46	4915.13	-0.33	2.7682	2.3	0.62	
	SiII*	1309.28	4934.02	...	...	...	<0.3	<0.1	
	SiII	1260.42	4749.84	4750.02	+0.18	2.7686	4.1	1.1	
	SiII*	1265.04	4767.30	...	...	...	<0.5	<0.15	
	SiII(2)	1193.28	4496.82	4496.74	-0.08	2.7684	2.3	0.62	
	SiII(1)	1190.42	4486.04	4486.05	+0.01	2.7685	1.5	0.40	
	SiII*	1197.42	4512.48	...	...	...	<0.5	<0.15	
	SiII*	1194.50	4501.47	...	...	...	<1.0	<0.25	
	SiIII	1206.51	4546.68	4546.09	-0.59	2.7680	3.8	1.0	
	SiIV(1)	1402.77	5286.27	5286.11	-0.16	2.7683	0.8	0.22	
	SiIV(2)	1393.76	5252.32	5252.09	-0.23	2.7683	1.7	0.44	
	FeII	1144.94	4314.65	4314.80	+0.15	2.7686	1.2	0.31	
					$\langle z_{abs} \rangle$ =	2.7685			

TABLE 5—*Continued*

	Ion	Rest λ (Å)	λ(1+z_{abs}) (Å)	Obs. λ (Å)	O-C (Å)	z_{abs}	W (Å)	W/(1+z) (Å)	Comments
"BEST BOGUS" Systems:									
4	MgI	2852.97	5262.98	5263.02	+0.04	0.8448	1.3	0.72	CIV λ1550 in z_{abs}=2.3938
	FeII	2600.18	4796.65	4797.25	+0.60	0.8450	1.5	0.82	
	FeII	2586.64	4771.68	4771.23	-0.44	0.8446	2.5	1.35	
	FeII	2382.76	4395.57	...	...	....	<0.6	<0.33	
	FeII	2344.21	4324.46	4324.44	-0.02	0.8447	3.0	1.64	
					$\langle z_{abs} \rangle$ = 0.8448				
5	HI	1215.67	5065.42	...	...	...	<1.0	<0.24	
	HI	1025.72	4273.94	4273.95	0.00	3.1668	1.0	0.24	
	SiII	1260.42	5251.88	5252.09	+0.21	3.1669	1.7	0.41	SiIV λ1393 in z_{abs}=2.7685
	SiII	1193.28	4972.15	4972.75	+0.60	3.1672	0.5	0.12	
	SiIV(1)	1402.77	5845.02	5844.82	-0.20	3.1666	2.2	0.53	CIV λ1550 in z_{abs}=2.7685
	SiIV(2)	1393.76	5807.48	...	...	...	<0.7	<0.17	
					$\langle z_{abs} \rangle$ = 3.1668				

from Si II are seen, but Si II λ1260 is blended with the strong Lα absorption in the system $z_{abs} = 2.7685$.

$z_{abs} = 2.7685$.—Another certain system with 16 lines, of which six are longward of Lα. The identification of the Fe II λ1144 line is questionable because of the lack of other available lines from this ion. The system is very similar in strength and line content to the $z_{abs} = 2.6381$ system.

We note that in the systems $z_{abs} = 2.6381$ and $z_{abs} = 2.7685$ the C II λ1334 line and the excited fine-structure line C II* λ1335 are both found in roughly equal strength in each case. They are in the region shortward of Lα emission, but the probability that both identifications are accidental is $\sim 10^{-2}$. On close inspection of the line profiles the C II* λ1335 line in the $z_{abs} = 2.6381$ system appears suspicious; however, the corresponding line in the $z_{abs} = 2.7685$ system is similar to the C II λ1334 line in both width and shape, thus adding weight to this identification. Furthermore, the separation of the lines is correct to within 0.25 Å.

In summary, the three redshift systems identify all 12 lines longward of the Lα emission line, but only 22 out of 101 of the lines shortward of Lα emission. This is typical of high-redshift QSOs.

b) Statistical Probabilities

In the previous section a description of the procedure used to search for and find redshift systems was given. We shall now describe how the reality of such systems is assessed. Our goal is to devise as straightforward and simple a method as possible that will effectively blitz "spurious" redshifts. This is done as follows:

1. Let Δ_J and Δ_L be the mean distances between lines shortward and longward of Lα emission, respectively. Choose an "acceptance window" $\Delta\lambda$ based on an assessment of the accuracy of the wavelength scale and quality of the data. Rather than use the $\sigma(\lambda)$ values for the lines as given in Table 3, we should keep $\Delta\lambda \geq 0.5$ Å. This allows for the possibility that different ions can have different systematic velocities within a given redshift. If one picks a random wavelength, then the probability that a line is within $\Delta\lambda$ of that point is $q_J = 2\Delta\lambda/\Delta_J$ or $q_L = 2\Delta\lambda/\Delta_L$ for lines shortward and longward of Lα, respectively.

2. An "expected line list" consists of the "short list" of Table 4. We delete from this list (*a*) lines which fall outside the observed wavelength region, (*b*) lines falling in blends or thickets of strong lines such that no decision can be made as to their presence or absence, and (*c*) lines expected to be below the equivalent width threshold based on the strongest lines from that ion. Note that (*c*) is ineffective against ions with only one available line.

3. Suppose we find J_1 of our expected lines shortward of Lα and fail to find J_2 of them. Similarly, if we locate L_1 lines longward of Lα but are missing L_2 of them, then we define

$$P(J_1, J_2; q_J) = \frac{(J_1 + J_2)!}{J_1! J_2!} q_J{}^{J_1}(1 - q_J)^{J_2},$$

which is just the binomial probability of J_1 successes and J_2 failures. Then the probability of $\geq J_1$ successes and $\geq L_1$ successes shortward and longward of Lα, respectively, is

$$Q = \sum_{m \geq J_1} P(m, J - m; q_J) \sum_{n \geq L_1} P(n, L - n; q_L),$$

where $J = J_1 + J_2$ and $L = L_1 + L_2$. The quantity Q is the basis probability that the system, at a single chosen redshift, could arise by chance.

4. Physical criteria are allowed for by the following simple rules. For doublets we multiply Q by one-half if the ratio of line strengths is ordered correctly. Further, a "doublet acceptance window" in wavelength, $\Delta\lambda^*$, has been prechosen after an assessment

of the accuracy of the wavelengths. Since systematic errors in the λ scale affect members of a close doublet equally, we choose $\Delta\lambda^* \leq \Delta\lambda$. If a doublet separation falls inside the window we multiply Q by $(\Delta\lambda^*/\Delta\lambda)[1 - (\Delta\lambda^*/4\Delta\lambda)]$ (the second factor allows for the fact that both lines can have wavelength residuals $\leq\Delta\lambda$ and yet the separation can be $\leq 2\Delta\lambda$; setting $\Delta\lambda = \Delta\lambda^*$ is more stringent than no test at all).

The strengths (W/λ) of the Fe II lines should be ordered as follows: $\lambda2382 > \lambda2600 > \lambda2344 > \lambda2586 > \lambda2374$. These orderings are valid for unsaturated lines (when $W \propto N_l\lambda^2 f$) and for saturated lines (when $W \propto \lambda \log_e(N_l f\lambda)$). If k lines are found and all k are ordered correctly, multiply Q by $r_{kk} = 1/k!$ If, at best, $(k - 1)$ can be ordered correctly, multiply Q by $r_{k,k-1} = [1 + (k - 1)^2]/k!$ and so on (r_{kl} = probability that $\geq l$ of the k lines can, *at best*, be ordered correctly if the line strengths are random).

The strengths of the Si II lines should be ordered thus: $\lambda1260 > \lambda1193 > \lambda1190 > \lambda1526 > \lambda1304$ (see Morton 1975). Apply a similar procedure as for Fe II.

If the product of all these factors is f, then we define $Q^* = fQ$. If the system does not satisfy physical criteria, then it is punished by having $Q^* = Q$. If all criteria are satisfied, then $Q^* \ll Q$.

5. It may be desirable to calculate the expected number of systems of the type in question that could arise by chance. The probability Q^* refers to the probability of a system arising by chance at a given, prechosen redshift. How many "trials" for such a system do we have in the QSO spectrum? Since the acceptance window for a line is of width $2\Delta\lambda$ (errors $\pm\Delta\lambda$) we have taken "trial" redshifts at intervals $\Delta\lambda$ through the spectrum. For "weak" systems (defined as having at most six lines) which would be seen only with lines longward of Lα emission we estimate $N_b = (\lambda_{max} - \lambda_{L\alpha})/\Delta\lambda$ trials. For "strong" systems ($\geq$ seven lines) which may be seen longward or shortward of Lα we take $N_b = (\lambda_{max} - \lambda_{min})/\Delta\lambda$. Here λ_{max}, λ_{min}, $\lambda_{L\alpha}$ are the edges of the observed region and the position of Lα emission, respectively. The expected number of spurious systems is then given by $N^* = N_b Q^*$. This expected number N^* refers to the number of spurious systems of the "ionic type" in question to be expected; it is *not* a measure of the number of systems of *any type* that would pass through our net.

To be convincing we require $N^* \ll N_{found}$, where N_{found} is the number of systems of our type which are found. The analysis of the three systems in PKS 2126−158 is given in Table 6. For $z_{abs} = 2.3938$ (which is the only dubious system), we note that of the lines available in the "short list" only C II $\lambda1334$ is not found. The lines Si II $\lambda\lambda1260,1304$ are deleted, since the former is in a region of poor signal-to-noise ratio and the latter is buried in a thicket. Si IV $\lambda1402$ is deleted, since the observed line at $\lambda4761.2$ (the correct position) is much too strong relative to $\lambda1393$; thus no decision about $\lambda1402$ can be made, it being buried in a blend. Thus $J_1 = 2$ (for Si II $\lambda1506$, Si IV $\lambda1393$), $J_2 = 1$ (for C II $\lambda1334$), $L_1 = 2$ (for C IV $\lambda\lambda1548, 1550$), and $L_2 = 0$. The strong line C IV $\lambda1548$ is confused, so no "good doublet" criteria are applied. The resulting N^* of 0.01 makes the system a reasonable possibility.

To test our method we have taken two bogus systems which were found in our computer search for redshifts. The line identifications are given in Table 5. Both systems (which were the redshifts next best to the three real ones) are deemed bogus by the values of N^* of order unity. Let us consider the system $z_{abs} = 3.1668$ in more detail. We have $L_1 = 2$ (for Si II $\lambda1260$, Si IV $\lambda1402$), $L_2 = 6$ (C IV $\lambda\lambda1548, 1550$, C II $\lambda1334$ Si II $\lambda\lambda1526, 1304$, Si IV $\lambda1393$ not found), $J_1 = 2$ (for H I $\lambda1025$, Si II $\lambda1193$), and $J_2 = 2$ (for H I $\lambda1215$, Si II $\lambda1190$ not found). Note we have been purposefully generous with this system. We should have struck out the identifications H I $\lambda1025$ (no Lα) and Si IV $\lambda1402$ (no Si IV $\lambda1393$) under rule 2(*c*). Further, the Si IV $\lambda1402$ line is identified in another, indisputable system (and should have been categorized "blended, no decision possible"). These liberties were permitted to illustrate the probabilities that would result from a similar system but with Lα instead of Lβ, etc., which would still receive a bogus rating. Similar generosity was meted out to $z_{abs} = 0.8447$, where the strongest Fe II $\lambda2382$ line is missing (and should have led to the deletion of all Fe II lines and the consequent collapse of the system).

Excision of bogus systems in this very effective manner results from:

1. Using high-resolution data which resolve blends and allow accurate wavelengths and small $\Delta\lambda$ acceptance windows. This was emphasized by Aaronson, McKee, and Weisheit (1975).

TABLE 6

PROBABILITY ANALYSIS OF REDSHIFT SYSTEMS

	z_{abs}	J_1	J_2	L_1	L_2	Q	Q*	N_b	N*
PKS 2126-158	2.3938	2	1	2	0	3.0×10^{-6}	3.0×10^{-6}	2700	8.1×10^{-3}
q_J = 0.1159	2.6381	6	1	3	0	1.3×10^{-11}	5.4×10^{-13}	4500	2.4×10^{-9}
q_L = 0.0088	2.7685	7	0	3	2	2.2×10^{-12}	8.0×10^{-14}	4500	3.6×10^{-10}
	0.8447†	3	3	1	0	2.2×10^{-4}	2.2×10^{-4}	2700	5.9×10^{-1}
	3.1668†	2	2	2	6	1.3×10^{-4}	1.3×10^{-4}	2700	3.5×10^{-1}

†Bogus systems to test analysis.

2. Using as short a line list as possible for identifications, based on strong lines in unimpeachable systems. If other lines establish themselves they can be added to the list.

3. Applying relative strength tests among each ion, and especially for doublets. No test for "plausible ionization conditions" (as in Aaronson, McKee, and Weisheit 1975) among different ions was conducted; with the quality of data presented here it was not necessary.

c) *Visibility Windows for Redshift Systems*

The ability to detect a redshift system is strongly dependent on z_{abs}, z_{em}, the observed wavelength region, and on the signal-to-noise ratio of the data. The most important effect is probably that the strongest lines usually observed (other than Lα) are C IV λλ1548, 1550 and Mg II λλ2796, 2803, and the likelihood of finding a given redshift is greatly increased when these doublets fall in the observed spectral region longward of the Lα emission line.

The resulting observational selection can be almost entirely eliminated by defining certain types of absorption-line systems which are required to fall in a certain visibility window before they are considered for statistical analysis. With suitable definitions, one can include most of the systems that are actually found in QSO spectra. We have defined four types of systems as follows (definitions are assigned after a system is accepted and are unrelated to the statistical analysis).

S_1 systems.—These are based on the appearance of the lines of H I λ1215, C II λ1334, C IV λλ1548, 1550, Si II λλ1190, 1193, 1260, 1304, 1526, Si III λ1206, and Si IV λλ1393, 1402; a total of 12 lines. We demand that at least eight lines must fall in the observed region and that at least seven of these must be visible, with $W_{rest} \geq 0.25$ Å (this is dictated by the regions of lowest signal-to-noise ratio in the data). If λ_{max} and λ_{min} are the edges of the observed region, then these restrictions imply $\lambda_{max} \geq 1393.76\ (1 + z_{abs})$ and $\lambda_{min} \leq 1260.42\ (1 + z_{abs})$, which defines a visiblity window for S_1 systems. For those limits to be valid, we require the observed spectral region to be sufficiently long that eight lines are guaranteed visible for a redshift in this "window." This occurs if $\lambda_{max} - \lambda_{min} > 341.69\ (1 + z_{abs})$ and is satisfied by our observations of PKS 2126−158. The definition of an S_1 system has been designed to be so restrictive that it can be detected even if all the lines occur shortward of Lα emission in the QSO.

W_1 systems.—These are weak versions of the S_1 systems and may only be found if most of the lines are longward of Lα emission in the QSO. We demand that the C IV doublet (with correct line strengths) must be visible longward of Lα emission and must have $W_{rest} \geq 0.25$ Å for both lines, and that at least one other line (H I, Si II, Si III, Si IV, C II) must be found in the system. Those restrictions imply that the edges of the visibility window are $\lambda_{max} \geq 1550.77\ (1 + z_{abs})$ and $\lambda_{L\alpha} \leq 1548.20\ (1 + z_{abs})$. Again, sufficient spectral coverage is required, with $\lambda_{L\alpha} - \lambda_{min} > 21.48\ (1 + z_{abs})$ and $\lambda_{max} - \lambda_{L\alpha} > 2.57\ (1 + z_{abs})$. Note that a system may be both W_1 and S_1.

S_2 systems.—The lines used to define these systems are Mg I λ2852, Mg II λλ2796, 2803, Fe II λλ2344, 2374, 2382,2600; a total of eight lines. The requirements for the S_2 systems are that at least five lines must be accessible, of which at least four must be visible with $W_{rest} \geq 0.5$ Å. The visibility window is $\lambda_{max} \geq 2600.18\ (1 + z_{abs})$ and $\lambda_{min} \leq 2586.64\ (1 + z_{abs})$, for the S_2 systems. The required spectral coverage is $\lambda_{max} - \lambda_{min} > 470.21\ (1 + z_{abs})$. These too might be found buried in the lines shortward of Lα.

W_2 systems.—In these the Mg II doublet is visible (with correct line strengths) and must fall longward of Lα emission with $W_{rest} \geq 0.5$ Å for both lines. At least one other line (Mg I, Fe II) must be found. Then, of course, $\lambda_{max} \geq 2803.52\ (1 + z_{abs})$ and $\lambda_{L\alpha} \leq 2796.35\ (1 + z_{abs})$. Again we should have $\lambda_{max} - \lambda_{L\alpha} > 7.18\ (1 + z_{abs})$, and $\lambda_{max} - \lambda_{min} > 252.79\ (1 + z_{abs})$ or $\lambda_{L\alpha} - \lambda_{min} > 196.17\ (1 + z_{abs})$. A system can be both S_2 and W_2.

Some rather obvious points about this scheme of classification are that, first, it removed most (but not all) of the selection effects in finding redshift systems if statistical analyses are done only with such classified systems. With the currently small samples of high-quality data this effect should not matter.

Moreover, one can compare number densities of each type of system in different QSOs having different redshift z_{em} and different observed wavelength regions with a minimum of bias. However, systems of different types (e.g., S_1 and S_2) cannot be intercompared for statistical purposes.

In Table 7 we give the visibility windows for the various types of system in PKS 2126−158. These definitions will be used in a forthcoming paper which includes data for other QSOs and addresses the question of the average density of the systems in QSO spectra, and their frequency of occurrence in different QSOs. Our method allows this to be done with a freedom from the observational selection effects which have plagued previous studies (e.g., Aaronson, McKee, and Weisheit 1975).

d) *Column Densities*

Our column density estimates for the three absorption-line systems are given in Table 8. We have assumed that the distribution of material along the line of sight is Gaussian, except for $z_{abs} = 2.6381$

TABLE 7

PKS 2126−158 ABSORPTION-LINE SYSTEM VISIBILITY WINDOWS

Type of System	No. of Systems	z_{min}	z_{max}	Δz
S_1.....	2	2.292	3.280	0.988
W_1.....	3	2.359	3.280	0.921
S_2.....	0	0.604	1.615	1.011
W_2.....	0	0.860	1.426	0.566
Others.....	0	...	...	...

TABLE 8

PKS 2126−158 ABSORPTION SYSTEM COLUMN DENSITIES

z_{abs}	2.3938		2.6381		2.7685
σ_v(km s^{-1})†	45	30:	25:	65	45
H I	...	...	1.1×10^{19}		1.1×10^{19}
C I	...	...	...	$< 7 \times 10^{13}$	$< 1.6 \times 10^{14}$
C II ($J = 1/2$)	...	...	5×10^{14}:	$< 2 \times 10^{14}$	1.3×10^{15}
C II* ($J = 3/2$)	...	...	(3×10^{14}:	3×10^{14})‡	4×10^{14}
C IV	3×10^{14}	...	...	5×10^{14}	5×10^{14}
O I	...	...	7×10^{14}:	$< 2 \times 10^{14}$	1.2×10^{15}
Al II	...	...	3×10^{13}:	$< 6 \times 10^{12}$	1.7×10^{13}
Si II ($J = 1/2$)§	...	$3 \times 10^{14} F_{1526}{}^{-1}$:	$4 \times 10^{14} F_{1526}{}^{-1}$:	$3 \times 10^{14} F_{1526}{}^{-1}$	1.8×10^{14}
Si II* ($J = 3/2$)	...	...	...	$< 2 \times 10^{13}$	$< 4 \times 10^{13}$
Si III	...	...	...	6×10^{13}	5×10^{14}
Si IV	2×10^{13}	...	...	7×10^{13}	6×10^{13}
Fe II	...	...	...	...	2×10^{14}

† The Doppler parameter b is related to σ_v by $b = \sigma_v\sqrt{2}$, thus $N(v) = A \exp(-v^2/2\sigma_v^2)$.

‡ Identification of C II* in this system is possibly bogus.

§ Oscillator strengths for this ion uncertain. $F_{1526} = f_{1526}/0.1$; f_{1526} = oscillator strength of λ1526.72.

where two Gaussians with different dispersions appeared to be necessary. Column densities were then calculated using an appropriate curve of growth for the various ionic species. In most cases it was clear that the lines were on the linear or logarithmic part of the curve of growth; in that case the tables of Strömgren (1948), which neglect damping, are satisfactory. The Lα lines are on the square-root part of the curve of growth; column densities $N_{\rm H\,I}$ were calculated for these lines by computing an appropriate curve of growth including the damping.

Multiple structure is sometimes seen in QSO absorption lines when observed at high resolution. In particular, there may be very low dispersion components with a high column density which have a small effect on the total equivalent width of the metal lines. The presence of such sharp components does not affect the *relative* column densities of the metals as calculated with the Gaussian distribution but can affect the derived H I–to–metal ratio.

The oscillator strengths tabulated for the Si II ions (Morton and Smith 1973) do not agree with observed line strengths (see, e.g., Morton 1975), and so we were unable to derive a satisfactory curve of growth for the Si II lines. Where the oscillator strengths are particularly suspect (e.g., Si II λ1526), we leave the explicit dependence in the column density. The column densities have been based on the Si II λλ1190, 1193 lines where possible, with the new f-values given in Morton (1978).

Some comments on the individual systems are as follows:

$z_{abs} = 2.3938$.—The C IV doublet ratio cannot be used to estimate the velocity dispersion σ_v because the stronger component is blended with Si IV λ1393 in the $z_{abs} = 2.7685$ system. We note that the C IV λ1550 and the Si IV λ1393 lines in this system are unsaturated (they are shallow while being considerably wider than the instrumental resolution) and we find $\sigma_v = 47$ km s^{-1} from C IV and $\sigma_v = 42$ km s^{-1} for Si IV. We adopt $\sigma_v = 45$ km s^{-1}. However, the width of the Si II λ1526 line is $\sigma_v = 29$ km s^{-1}, and the line is deep enough to be beginning to saturate. Indeed, it is not clear whether the failure of the line to drop to zero intensity (after correcting for instrumental resolution) is because it is not completely saturated or because the cloud does not completely cover the QSO emission-line region (the Si II λ1526 line is embedded in the Lα emission). An estimate of the column density is given, however, using $\sigma_v = 30$ km s^{-1} and assuming it does cover the QSO emission-line region.

$z_{abs} = 2.6381$.—This system exhibits two components of different dispersions with no systematic velocity difference. An examination of the C IV λλ1548, 1550 and Si II λ1526 lines shows a broad plus narrow component structure, hints of which are also seen in the Si IV λλ1393, 1402 lines. The O I λ1302 and Al II λ1670 lines show the narrow component only, as do the C II λ1334, Si II λλ1190, 1304 lines, although the last three are partly blended. The Si III λ1206 line shows the broad component only.

The dispersion σ_v for the broad system may be obtained from the C IV doublet ratio, after removing the equivalent-width contribution from the narrow components. The ratio R(C IV) = 1.46 leads to a dispersion $\sigma_v = 63$ km s^{-1}, which is in accord with the width of the Si III λ1206 and the broad component of the Si II λ1526 lines. These lines yield upper limits on σ_v of 75 and 80 km s^{-1}, respectively. Accordingly, we take $\sigma_v = 65$ km s^{-1}. With this dispersion we calculate the column density in the broad components of C IV, Si IV, Si III, Si II, and C II*, and give upper limits for C II, O I, and Al II. The presence of a narrow, central component has little effect on the equivalent width of the broad component, after removing the central deep core, unless the narrow line is damped and contributes to the wings (however, none of the lines show strong Lorentzian wings, as would be expected in this case).

The velocity dispersion of the narrow system is difficult to evaluate; in particular, it is difficult to see whether different ions have the same dispersion or not. Upper limits from the Al II λ1670 and Si II λ1526 lines

are 26 and 25 km s^{-1}, respectively; both lines are saturated, since they reach zero intensity in the center (after allowing for instrumental resolution). We *assumed* a dispersion $\sigma_v = 25$ km s^{-1} and calculated the column densities with this value. Strictly, these values are lower limits. The column densities for C IV and Si IV are not given because it is not possible to extract a reliable equivalent width for the narrower component in those lines. Inspection of the C IV doublet shows the narrow components equally deep and reaching zero intensity if the instrumental resolution is allowed for. This shows that the narrow component is saturated in C IV, which requires a column density of at least 5×10^{14} cm^{-2} when $\sigma_v = 25$ km s^{-1}.

$z_{abs} = 2.7685$.—There is no evidence for multiple structure in the lines of this system. However, the C IV λλ1548,1550 doublet ratios are measured from two different observations disagree seriously (see Fig. 1). Taking the mean value R(C IV) = 1.45 leads to a dispersion $\sigma_v = 51$ km s^{-1}. The Si II λλ1190,1193 doublet has a ratio R(Si II) = 1.53 and gives $\sigma_v = 55$ km s^{-1}. The errors on both these ratios would admit values less than $\sqrt{2}$ when the solution is double-valued, but examination of the line profiles fails to show the strong wings expected of the damped solution. Finally, upper limits on σ_v from Si II λ1526 and Si IV λ1402 are 41 and 45 km s^{-1}, respectively. Thus the low and high ionization states seem to have the same dispersion, and we shall adopt $\sigma_v = 45$ km s^{-1} for all lines.

The resulting column densities are given in Table 8. We used the Si II λ1190 line to calculate the N(Si II) column density, and the damping formula for N(H I). We particularly note the ratios N(C II*)/N(C II) = 0.31, N(Si II*)/N(Si II) < 0.22, and the large value of N(Si III) as compared with Si II and Si IV. This, however, may be spurious if the Si III λ1206 is blended.

IV. THE Lα ABSORPTION LINES

As discussed in § III*a* only 22 lines shortward of Lα emission in PKS 2126−158 were identified, leaving 79 unidentified lines. These cannot be unidentified C IV or Mg II doublets for the following reasons. We have found three C IV doublets longward of Lα in a region of length 1400 Å, and so ~2 doublets may be expected in the 1000 Å covered shortward of Lα emission. In Figure 3 we have plotted the distribution of line pairs with a specified separation $\Delta \ln (1 + z) = |\ln (\lambda_1/\lambda_2)|$ (among the unidentified lines) in the spectrum of PKS 2126−158. This includes all line pairs, not merely adjacent lines. Also marked on Figure 3 are the wavelength ratios of the strongest line pairs we expect to find in QSO absorption spectra. No significant peaks are evident in the distribution, implying that at most three C IV or Mg II doublets are present shortward of Lα emission.

The observed spectrum of PKS 2126−158 extends 230 Å in the rest frame shortward of Lβ emission. We have plotted the distribution of line pairs among the unidentified lines around the Lα/β ratio, as is shown in Figure 4. No significant peak occurs at the Lα/β ratio, showing that at most two Lα/β pairs exist in the spectrum. In Table 9 we examine each line shortward of Lβ emission in the QSO and look for a corresponding Lα. As can be seen after examination of wavelength errors and equivalent widths, there are only three even possible Lα–Lβ pairs remaining.

In fact, it is not surprising that we should fail to find the Lα/β pairs. The typical postulated Lα lines have $W_\alpha = 2$ Å, and so if it is on the linear part of the curve of growth, the strength of the corresponding Lβ line is expected to be only $W_\beta = 0.3$ Å. This is a factor of 3 below being detectable, since the region of spectrum containing Lβ has a poor signal-to-noise ratio.

If the majority of the Lβ lines are a little below the

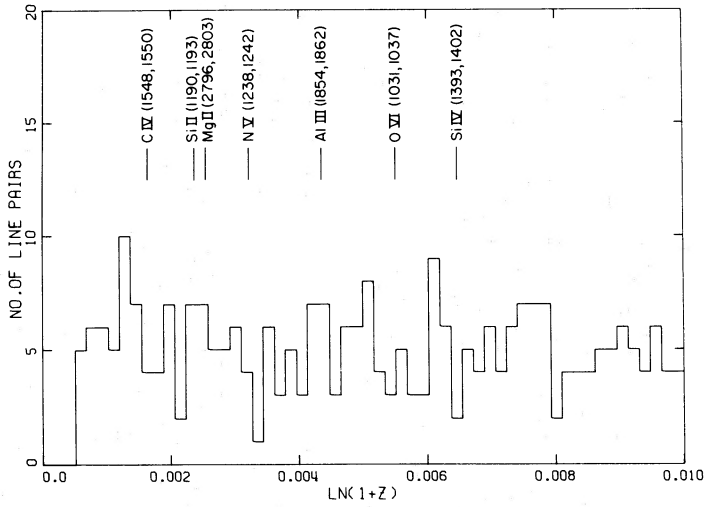

FIG. 3.—Distribution of splittings $\Delta \ln (1 + z) = |\ln (\lambda_1/\lambda_2)|$ among pairs of unidentified absorption lines in the spectrum of PKS 2126−158. The positions of seven pairs, expected in QSO spectra, are marked.

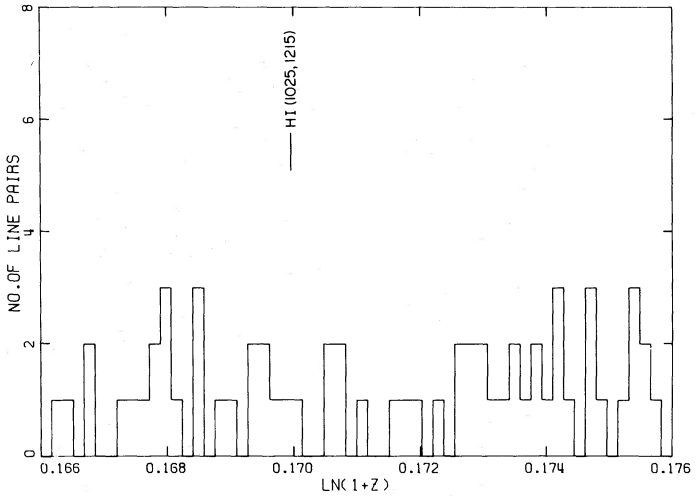

FIG. 4.—Distribution of splitting $\Delta \ln (1 + z) = |\ln (\lambda_1/\lambda_2)|$ among pairs of unidentified lines in PKS 2126 − 158. This shows the region around the splitting $\Delta \ln (1 + z) = 0.1699$ of Lα–Lβ pairs.

detectable limit, then we may find evidence for their existence by cross-correlating the Lβ region with the Lα region of the spectrum. This has been done in two cases. First, Figure 5 shows a raw cross-correlation between the Lα region from 4922 Å to 5203 Å and the Lβ region from 4153 Å to 4390 Å. A peak is evident at the correct Lα/β ratio, but is surrounded by peaks of similar height. These latter peaks are caused by accidental meshing of strong lines in the two regions of spectrum. To test this idea, Figure 6 shows a cross-correlation in which all the strong lines in the Lβ region have been removed and replaced with a mean continuum level. The Lα/β peak seen in Figure 5 is undiminished and is now the only strong peak present.

If we normalize the height of the continuum of the spectra to unity, and also normalize the total length to unity, we may calculate the value of the correlation function, C, of the spectra (with $C = 1$ resulting if both are featureless). Approximate a Lα line as being a rectangle of depth D and width W, and a corresponding Lβ line as having depth D' and width W. Then the height of the correlation peak is the difference in the correlation function values which result when the lines are "meshed" and "not meshed." This is, simply,

$$\Delta C = WDD'[1 - 2W + W(D + D')]^{-1} .$$

The factor in square brackets normalizes C to unity when the lines are "unmeshed" (as was done in calcu-

TABLE 9

Lα—Lβ PAIRS IN PKS 2126−158

No.	λ_β	W_β	$\lambda(1+z_{\alpha\beta})=\lambda_\alpha$	λ_α'	W_α'	Remarks
1	4156.4	1.6	4926.1	...	...	
2	4175.9	4.4	4949.2	...	...	
3	4197.2	2.1	4974.5	4972.8	0.5	
4	4205.3	3.8	4984.1	4982.7	1.9	
5	4211.2	2.0	4991.1	...	...	
6	4234.7	2.2	5018.9	5018.5	1.8	Possible
7	4237.8	2.9	5022.6	...	...	
8	4240.6	1.0	5025.9	...	...	
9	4243.3	2.2	5029.1	5028.8*	3.0	
10	4274.0	1.0	5065.5	5064.4	1.9	Possible
11	4283.6	4.3	5076.9	...	...	
12	4295.0	1.1	5090.4	...	...	
13	4300.5	1.8	5096.9	...	...	
14	4314.8*	1.2	5113.8	...	...	
15	4320.9	3.1	5121.1	...	...	
16	4324.4	3.0	5125.2	5125.8	2.9	Possible
17	4327.3	0.9	5128.7	...	...	
18	4331.1*	2.0	5133.2	5135.0	1.8	
19	4339.9*	4.9	5143.6	5143.5	1.6	
20	4360.4	1.5	5167.9	...	...	
21	4382.5	1.1	5194.1	...	...	
22	4389.9*	2.7	5202.9	...	...	

*Identified metal line.

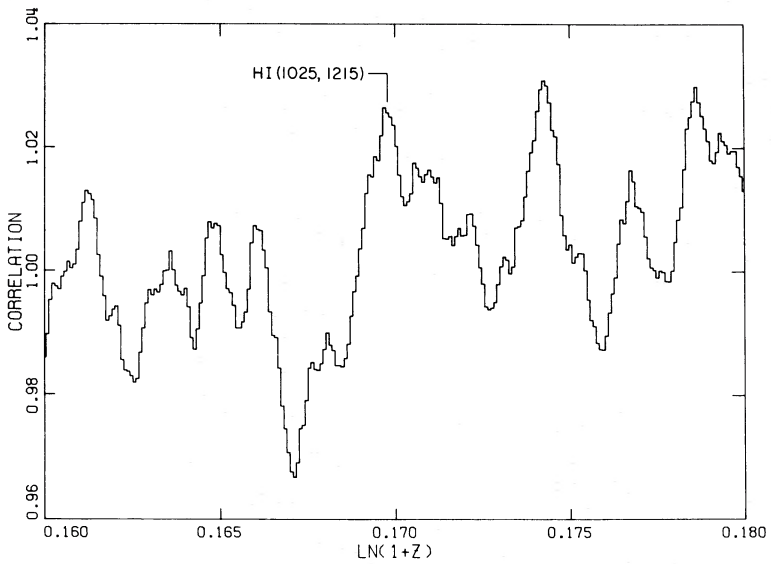

FIG. 5.—Correlation function between segments of spectrum of PKS 2126−158 to the blue of Lα and of Lβ emission. The point at which Lα–Lβ lines in the same redshift are coincident is marked.

lating the functions in Figs. 5 and 6). The height of the peak is unchanged if the large rectangular lines representing Lα and Lβ are split up into many narrower ones, provided the lines in corresponding Lα–Lβ pairs have the same widths (however, the width of the correlation peak becomes narrower). For the Lα lines in PKS 2126−158 we find $W = 0.22$, $D = 0.8$. For corresponding Lβ lines where both Lα and Lβ are optically thin we find $D' = 0.11$. Then $\Delta C = 0.025$, which is just the height of the peak corresponding to Lα/β that we have found. If two strong lines should mesh, with $D = D' = 1$ and $W = 0.02$, we find $\Delta C = 0.02$ again in accord with the size of the peaks in Figure 5. The width of the Lα/β peak is 3 Å, which is the typical FWHM of the supposed Lα lines.

These considerations strongly suggest that most of the absorption equivalent width (i.e., lines) shortward of Lα emission is indeed Lα absorption. We require $\gtrsim 90\%$ of the unidentified lines in the region which was cross-correlated to be Lα in order to explain the strength of the peaks in Figures 5 and 6.

V. CONCLUSIONS

Our main conclusions are as follows:

1. We presented a list of 113 absorption lines in the spectrum of PKS 2126−158 ($z_{em} = 3.280$), in the

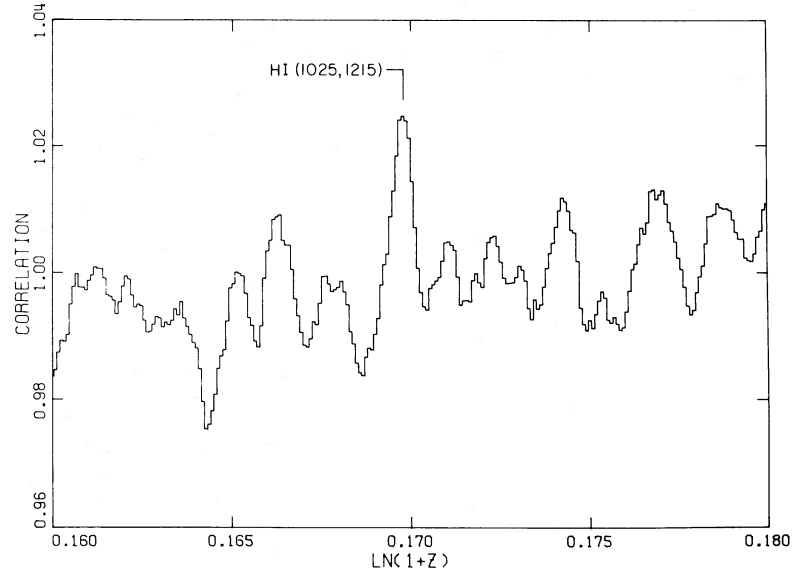

FIG. 6.—Correlation function between Lα and Lβ regions of PKS 2126−158 spectrum. Here the strong lines in the Lβ region have been removed (by replacing them with "continuum"). The Lα–Lβ separation, $\Delta \ln(1 + z) = 0.1699$, is marked.

range λλ4153–6807. Heliocentric, vacuum wavelengths, and equivalent widths are given in Table 3.

2. We established two certain absorption redshift systems at $z_{abs} = 2.6381$ (14 lines) and $z_{abs} = 2.7685$ (16 lines). A further possible system resides at $z_{abs} = 2.3938$ (four lines). These systems were all proposed earlier by Jauncy *et al.* (1978*a*, *b*). A measure of the reality of each system was calculated.

3. Estimates of column densities were obtained for the ions present in the redshift systems. Of the fine-structure states, Si II* ($J = 3/2$) is absent from all systems. C II*($J = 3/2$) is almost certainly present in the $z_{abs} = 2.7685$ system.

4. The selection effects present in finding redshift systems were discussed. A scheme has been established which, by making use of well-defined criteria for specific types of redshift system, largely eliminates selection effects and allows uniform probability of discovery over a given, well-defined visibility window.

5. We examined the many unidentified lines shortward of Lα emission. Although at most three Lα/β pairs are visible in the spectrum, a cross-correlation analysis shows $\gtrsim 90\%$ of the unidentified lines must be single Lα lines.

We thank D. Jauncey and B. Peterson for telling us of their identification of PKS 2126−158 during our observing run. We are grateful to the UK Panel for Allocation of Telescope Time for the generous allotment of time which made the observations possible, and for financial support. The development of the IPCS was financed with the aid of grants from the UK Science Research Council. We thank an anonymous referee for many valuable comments which corrected several errors and resulted in a significant clarification of this work. W. S. thanks the National Science Foundation for a Travel Grant in order to assist in the observations. Other work by W. S. and P. J Y. was supported by National Science foundation grant AST 75-00555.

REFERENCES

Aaronson, M., McKee, C. F., and Weisheit, J. C. 1975, *Ap. J.*, **198**, 13.
Bahcall, J. N. 1968, *Ap. J.*, **153**,.679.
Baldwin, J. A. 1977, *Ap. J.*, **214**, 679.
Boksenberg, A. 1972, in *Auxiliary Instrumentation for Large Telescopes*, ed. S. Lausten and R. Reiz (ESO-CERN), p. 295.
Jauncey, D. L., Wright, A. E., Peterson, B. A., and Condon, J. J. 1978*a*, *Ap. J.* (*Letters*), **219**, L1.
———. 1978*b*, *Ap. J.* (*Letters*), **223**, L1.
Lynds, C. R. 1971, *Ap. J.* (*Letters*), **164**, L73.
Morton, D. C. 1975, *Ap. J.*, **197**, 85.
———. 1978, *Ap. J.*, **222**, 863.
Morton, D. C., and Smith, W. H. 1973, *Ap. J. Suppl.*, **26**, 333.
Sargent, W. L. W., Young, P. J, Boksenberg, A., Shortridge, K., Lynds, C. R., and Hartwick, F. D. A. 1978, *Ap. J.*, **221**, 731.
Smith, M. G. 1975, *Ap. J.*, **202**, 591.
Strömgren, B. 1948, *Ap. J.*, **108**, 242.

Note added in proof.—Line 71 in Tables 3 and 5 is at redshift $z = 2.6383$. Line 86 in Tables 3 and 5 is at $z = 2.7684$. Line 101 in Table 3 is at $z = 2.3938$.

A. BOKSENBERG: Department of Physics and Astronomy, University College London, Gower Street, London WC1E 6BT, England

R. F. CARSWELL and J. A. J. WHELAN: Institute of Astronomy, Madingley Road, Cambridge CB3 0HA, England

WALLACE L. W. SARGENT and PETER J YOUNG: Department of Astronomy 105–24, California Institute of Technology, Pasadena, CA 91125